

# A Neutron Sensitive Detector Using 3D-Printed Scintillators

---

A. Barr,<sup>a</sup> C. Da Vià,<sup>a,b</sup> M.T. Binte Shawkat,<sup>a</sup> M.J. Taylor,<sup>a</sup> S. Watts,<sup>a</sup> J. Allison,<sup>a</sup> G. D'Amen,<sup>c</sup>

<sup>a</sup>*University of Manchester,  
Oxford Road, United Kingdom*

<sup>b</sup>*Stony Brook University,  
100 Nicolls Road, United States of America*

<sup>c</sup>*Brookhaven National Laboratory,  
98 Rochester Street, United States of America*

E-mail: [adam.barr@manchester.ac.uk](mailto:adam.barr@manchester.ac.uk)

**ABSTRACT:** This work reports on the performance of a novel neutron-sensitive scintillating detector fabricated using Fused-Deposition Modelling (FDM) additive manufacturing. FDM is a cost-effective 3D-printing method employing flexible plastic filaments to create custom-shaped components. Scintillating filaments, based on polystyrene doped with *p*-terphenyl and 1,4-bis(5-phenyloxazol-2-yl) benzene, and enriched with <sup>6</sup>LiF to enable neutron sensitivity were manufactured in house and achieved visible scintillation with a light output of  $30 \pm 5$  photons per MeV. Printed scintillators were then integrated into a detector system consisting of an image intensified TimePix3 camera, offering high spatial and temporal resolution. The detector performance was compared with Geant4 simulations of the scintillating sensor's response to electrons, gamma-rays, and thermal neutrons. A novel event discrimination algorithm, using the properties of the TimePix3 camera, enabled the separation of neutron signatures from the gamma-ray background.

**KEYWORDS:** Scintillators, scintillation and light emission processes (solid, gas and liquid scintillators); Neutron detectors (cold, thermal, fast neutrons); Scintillators and scintillating fibres and light guides; Search for radioactive and fissile materials

---

## Contents

<b>1</b>	<b>Introduction</b>	<b>1</b>
<b>2</b>	<b>Plastic Scintillators</b>	<b>2</b>
2.1	Production of Scintillating Materials	2
2.2	Additive Manufacturing of Scintillators	3
<b>3</b>	<b>Neutron Detection</b>	<b>3</b>
<b>4</b>	<b>3D-Printing Neutron-Sensitive Scintillators</b>	<b>4</b>
4.1	Filament Production	4
4.2	3D-Printing Process	5
4.3	Detector Integration	7
<b>5</b>	<b>Detector Performance</b>	<b>7</b>
5.1	Neutron-Gamma Discrimination	8
<b>6</b>	<b>Conclusions</b>	<b>11</b>

---

## 1 Introduction

Scintillators are a widely used solution for detecting radiation, offering high flexibility and a broad range of applications. The first plastic scintillator, polystyrene doped with *m*-terphenyl, was discovered by Schorr and Torney in 1950 [1]. Since then, a large variety scintillating materials have been discovered and used in particle physics, medicine, biology and other scientific fields in combination with visible light detectors [2].

The popularity of plastic scintillators is mainly due to their good light outputs combined with a rapid decay time making them highly suitable for particle identification. While many scintillators are composed of low-*Z* elements (mainly carbon and hydrogen), they could easily be combined with high-*Z*<sub>eff</sub> materials to enable effective gamma-ray spectroscopy [3]. When layered with high-*Z* materials, scintillating materials have been used effectively for calorimetry [4]. Segmented designs have also been used for particle tracking with submillimeter resolution [5].

Neutron-sensitive scintillators form a particular area of interest, with both scientific and commercial applications, for example in neutrino physics. Inverse beta decay, described by the following equation

$$\bar{\nu}_e + p \rightarrow n + e^+, \quad (1.1)$$

sees both a neutron and a positron being produced [6]. In a scintillator with a short decay time, the time difference between the prompt scintillation light from the positron capture and delayed light from the neutron capture gives a clear signature of neutrino detection; this is a role to which

plastic scintillators are well suited. Neutron-sensitive plastic scintillators have also found important applications in nuclear security and forensics. Neutrons are a key signature of fissile materials' decay, and their presence could pose major security threats if used for aggressive purposes; for this reason, there is extensive interest in neutron detection for homeland security and non proliferation (e.g. [7–9]). Furthermore, the resilience of plastic scintillators to changes in temperature and humidity allows their use in a wide variety of climatic conditions such as ports and countries border crossings [2].

Maximizing the performance of plastic scintillators often demands complex geometries, which are difficult to achieve using traditional manufacturing techniques. In this article, we present a more versatile approach based on additive manufacturing for producing neutron-sensitive plastic scintillators. We also detail strategies to integrate these scintillators into a functional detector system employing a fast optical camera.

## 2 Plastic Scintillators

Most plastic scintillators exploit one of two main polymers: poly-vinyl toluene (PVT) or polystyrene (PS). These have very short attenuation lengths for optical photons, so must be combined with wavelength-shifting dyes. Several of these fluorophores are in common use, with *p*-terphenyl (PTP), 2,5-diphenyloxazole (PPO), naphthalene and 1,4-bis(5-phenyl-2-oxazolyl)benzene (POPOP) being commonly used [2]. While new plastics and fluorophores are continually being tested, few have been able to supplant these well-understood materials.

Plastic scintillators have a well-understood mechanism of operation. The plastic can be understood as a matrix of polymers. Energetic charged particles entering the scintillator excite this matrix. The Foerster mechanism, a resonant dipole-dipole interaction, transfers this excitation to a primary fluorophore, such as PTP [10]. This nonradiative transfer depends heavily on the intramolecular distance. Once excited, the primary fluorophore emits photons. The attenuation length for scintillators with only a primary fluorophore is typically too low to be useful, less than 10 cm [2]. To avoid this, a secondary fluorophore, such as POPOP, is added. This absorbs photons emitted by the primary fluorophore and re-emits them at a more suitable wavelength [11]. This also allows the emission wavelength of the scintillator to be tuned to meet the requirements of the photo-multiplier tube (PMT), silicon photo-multiplier (SiPM) or camera used to observe it. However, most secondary fluorophores emit in the blue band, so detectors should be sensitive to this band.

### 2.1 Production of Scintillating Materials

The fabrication of plastic scintillators usually starts with bulk monomers, primarily styrene or vinyl-toluene. These are heated to induce polymerization. If fluorophores are added to the monomers before heating, the resulting liquid polymer can be poured into moulds and cast to form a scintillator [2]. This produces a block of high-quality scintillator, but the equipment required is expensive and the process requires careful temperature control.

Another option is to use granules of the base polymer combined with the fluorophores. When heated above the glass transition temperature of the polymer, they can be made to flow. The plastic can then be injected into a mould, or extruded through a nozzle [12, 13]. This produces lower-quality

scintillators, but at much lower cost. As such, these methods are commonly used in the production of large-scale detectors.

These traditional methods have several issues. They require expensive industrial equipment to heat and cast, mould or extrude the plastic. The shape of the scintillator cannot easily be changed. These methods tend to produce blocks or cylinders of a fixed size, which must then be worked to the required shape using subtractive methods like cutting or drilling. The composition of a scintillator is fixed by the manufacturer and cannot be easily changed to suit a particular application.

## 2.2 Additive Manufacturing of Scintillators

Additive manufacturing, or 3D-printing, offers a way to solve the problems outlined in Section 2.1. It allows users to cheaply and rapidly produce scintillators in a scalable manner, and enables easy customization of the composition, internal geometry and external geometry of the scintillator. This is particularly true for plastic scintillators, which can be produced using off-the-shelf equipment. Two main methods have previously been used to 3D-print scintillators: stereolithography (SLA) and fused deposition modelling (FDM) [14, 15]. Both work on the basic principle of building up a piece, layer by layer. In SLA, an ultraviolet (UV) laser is used to selectively cure a liquid resin. This method allows for easy inclusion of additives such as dyes, fluorophores or neutron-sensitive isotopes. It also offers a high printing resolution, with the smallest feature possible being set by the size of the UV laser spot. However, it can only be used with a limited subset of plastics; the resins that can be used also pose a significant health hazard.

The simplicity with which additives can be integrated into SLA printing methods has made it a focal area for research into 3D-printed scintillators. Mishnayot et al. [16] used a combination of PPO, POPOP and naphthalene in a curable resin to obtain an effective printable scintillator. More recently, Kim et al. [17] have successfully printed PVT-based scintillators using SLA, obtaining very good results. Stowell et al. [18] have used SLA techniques to manufacture a neutron-sensitive scintillator, using boron nitride and zinc sulfide in an inert matrix.

FDM, meanwhile, extrudes a thermoplastic filament through a heated nozzle. FDM printing can be used with a wider variety of plastics than SLA, enabling the direct printing of scintillators without additives. It also allows multiple materials or filaments to be printed together. FDM printers are also available at lower cost. The production of customized filaments requires a separate system; as a result, its use for scintillators has been explored less thoroughly than the use of SLA. Early experiments by Hamel and Leboutellier [19] used poly-lactic acid doped with PPO and 1,4-Bis (2-methylstyryl) benzene (bis-MSB) to print scintillators, to moderate results. More successfully, Berns et al. [20, 21] have demonstrated the ability to print a polystyrene-based scintillator with FDM, while Sibilieva et al. [22] have used FDM to print inorganic scintillators in a plastic matrix. The work of Berns et al. has recently been extended by Li et al. [23], using FDM to produce a segmented detector for particle tracking.

## 3 Neutron Detection

Neutrons are difficult to detect directly. Instead, indirect methods have to be used. One option is to use activation foils, made from isotopes that will be transmuted to a radioactive isotope when they absorb a neutron [24]. By measuring the radiation output from these foils post-exposure to a neutron

source, the neutron flux from the source can be inferred. This is an effective, and easy-to-implement method, but does not allow for real-time measurements of the source flux. A more real-time method is to measure protons recoiling from neutron impact [25]. This requires the use of a material with a large proportion of hydrogen, making it suitable for use with plastic scintillators. However, the proton signal can be hard to distinguish from gamma rays and other forms of radiation, limiting its utility.

The most flexible option is to dope a detector with isotopes like  ${}^3\text{He}$ ,  ${}^{10}\text{B}$  or  ${}^6\text{Li}$ , which have a high neutron interaction cross-section [26]. Neutron reactions with these nuclei will release charged particles which can then be detected by conventional means, such as scintillators. For this experiment, we will focus on  ${}^6\text{Li}$ , which has a typical abundance of 7.6% in natural lithium. A neutron reaction with  ${}^6\text{Li}$  will release a tritium nucleus and an alpha particle, according to the following equation.



This reaction produces 4.78 MeV of energy, which is divided between the two reaction products, with  $E_{{}^3\text{H}} = 2.73$  MeV and  $E_{\alpha} = 2.05$  MeV [27]. This energy is considerably higher than that from  ${}^{10}\text{B}$  reactions [2]. It also produces an alpha particle rather than a gamma-ray, meaning that the scintillator light will be emitted close to the interaction. For thermal neutrons, the cross-section of this reaction is 940 barns, giving a strong sensitivity to thermal neutrons. Lithium compounds can easily be integrated into a scintillator, making this interaction a highly suitable method for producing a neutron-sensitive plastic scintillator.

## 4 3D-Printing Neutron-Sensitive Scintillators

We selected FDM for this project, as it is compatible with a wide range of materials. A number of FDM-compatible plastics are effective scintillators, including polyethylene terephthalate. However, following the example of Berns et. al (2020) [20], polystyrene was chosen as the base material for the filament. Polystyrene is well suited to FDM as it has a highly suitable glass transition temperature of  $\sim 100^\circ\text{C}$  and a high melt flow index at FDM temperatures [28]. It is well understood as a plastic scintillator, and is well-suited to particle detection, having high transparency, short decay times and a high light output for a plastic scintillator.

### 4.1 Filament Production

The polystyrene was combined with PTP as a primary fluorophore and POPOP as a secondary fluorophore, with 2% of the former and 0.05% of the latter being found to give maximum light output. A pure polystyrene filament proved to be too brittle to effectively 3D-print. It would snap when exposed to the rapid movements of the print head, or be crushed in the extruder, leading to print jams. To increase the flexibility of the filament, a plasticizer was added. Biphenyl, which dissolves well in polystyrene, was chosen. The minimum necessary biphenyl content was found to be 7.5%, which gave the flexibility required to print effectively without significant impact on light output. Finally, to allow the scintillator to detect neutrons, 0.1% by weight of  ${}^6\text{Li}$  was added to the material, in the form of  ${}^6\text{LiF}$  powder. All materials were procured from Sigma Aldrich.

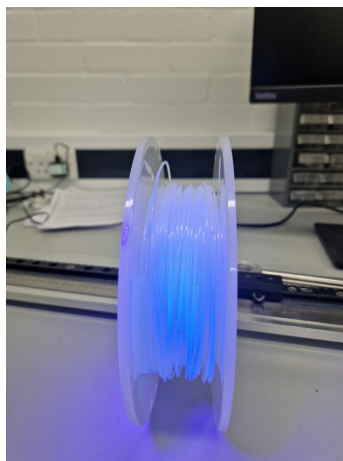


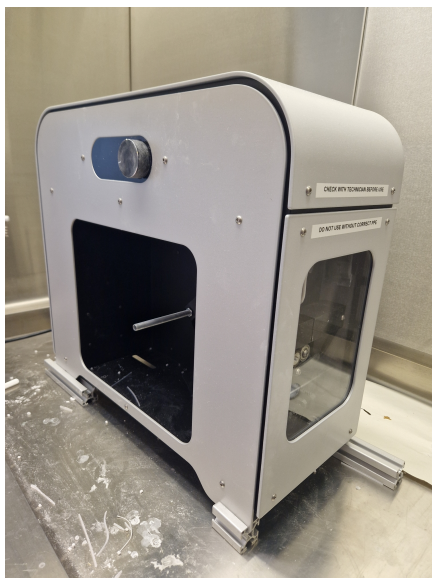
**Figure 1:** A reel of lithium-containing scintillating filament, fluorescing under UV light

These components were added to the intake hopper of a 3devo Composer filament maker [29], which mixed them and extruded the filament. The filament was extruded in 100 g reels, which could then be printed. An example of one of these reels can be seen in Figure 1. The filament maker, meanwhile, can be seen in Figure 2a. The intake hopper required constant agitation, both to effectively mix the powdered components with the polystyrene pellets and to prevent components with a low melting point from forming a plug which would jam the intake. The filament was extruded using an average temperature of 230° C, at a low speed to ensure adequate cooling of the filament as it was extruded. The 3devo Composer controls the diameter of the filament by controlling the rate at which the filament is drawn through a broad nozzle; this makes it easier to extrude filaments for multiple 3D-printers, which require different filament diameters. For this experiment, only a 1.75 mm diameter filament was produced.

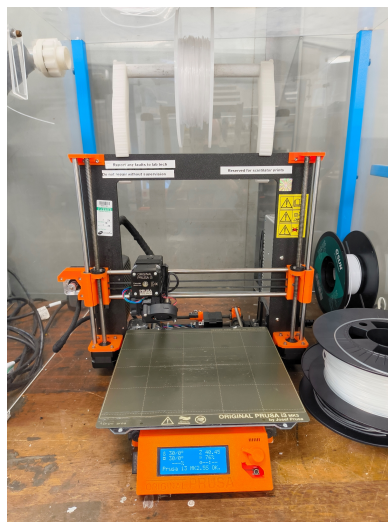
## 4.2 3D-Printing Process

The filament obtained, as described in Section 4.1, was printed using a Prusa i3 3D-printer [30], as seen in Figure 2b. Most 3D-printed objects use a shell around an infill structure. However, this is unsuitable for printing transparent objects like scintillators, as the infill structure traps gas bubbles. To avoid this, the printing parameters had to be modified to ensure maximum transparency. 100% infill was selected, to ensure that the final scintillator was filled completely with plastic. To reduce surface roughness, especially on the sides, a layer height of 0.05 mm was selected. The infill layers were also directly aligned, to minimise gas bubbles. There is a strong relationship between printing temperature and transparency, with higher temperatures producing a more transparent scintillator. However, higher temperatures also reduce the shape accuracy of the printing, as the plastic can more easily flow before cooling. A print temperature of 255° C, with no cooling of the print, was found to give the highest transparency while retaining acceptable shape tolerances. To ensure the extruded plastic had time to fill all space on the layer below, the print speed was set to 12 mms<sup>-1</sup>, 20% of the basic setting. The flow rate was also increased, to 112% of the base flow rate. This combination of settings was found to give an effectively transparent scintillator. However, there were imperfections in the printing of some scintillators, caused by the presence of gas bubbles, or





(a) The 3Devo Composer Filament Maker.



(b) The Prusa i3 3D-printer.

**Figure 2:** Figure 2a shows the filament maker used to produce neutron-sensitive 3D-printer filament, with a diameter of 1.75 mm. The filament is then used to print scintillators using the 3D-printer seen in Figure 2b

by underextrusion. This was due to inconsistencies in the diameter of the filament. Using a filament extruder with a fixed 1.75 mm nozzle, would avoid this issue.

After the completion of the 3D-printing process, the scintillator required post-processing to remove roughness caused by the FDM printing process on the external surfaces of the finished part. Additionally, the high printing temperature and high flow rates leave excess plastic on the edges of the printed scintillator. To ensure the print was fully transparent, any excess material was trimmed off, before sanding and polishing. While this reduces the size of the finished scintillator, the polishing process greatly enhances transparency. Accounting for the post-processing requirement, as well as the lack of accurate shape control that results from the high-transparency printing process, the scintillators could be printed to a tolerance of 0.3 mm. A printed and polished scintillator can be seen in Figure 3. An alternate method to smooth the surface of the scintillator, by exposing it to acetone vapour, was tested. This produced smooth, transparent scintillators that maintained a higher shape tolerance. However, over several days they became cloudy, as residual acetone vapour infiltrated into the interior of the scintillator. Vapour smoothing was also inconsistent; on several pieces, a layer of bubbles formed on the exposed surfaces of the scintillator, resulting in low transparency.

Scintillators were printed in a variety of shapes and thicknesses. While all displayed sensitivity to  $\alpha$ ,  $\beta$  and  $\gamma$  radiation, low sensitivity to neutrons was observed. Simulations indicated that this was due to low lithium content. However, increasing the lithium content would result in decreased transparency, reducing effective light output for a single-material scintillator. This was achieved by printing a two-part scintillator, with a cavity in the centre. This cavity could be packed with  ${}^6\text{LiF}$  powder, increasing the lithium content of the scintillator, but retaining high transparency.



**Figure 3:** An example of a lithium-containing 3D-printed scintillator; in this case, a 2 cm by 2 cm by 0.5 cm cuboid.

### 4.3 Detector Integration

Once a satisfactory scintillator was obtained, it could be integrated into a detector system based on an Amsterdam Scientific Instruments TPX3Cam, a fast optical camera based on the TimePix3 (TPX3) readout chip [31]. TimePix3 is an application specific integrated circuit (ASIC) which enables rapid readout of data at high bandwidth, it is bonded to a  $256 \times 256$  pixel high quantum-efficiency optical sensor [32]. The spatial resolution of the camera is  $\sim 16 \mu\text{m}$  and the temporal resolution is 1.56 ns [33]. The TPX3Cam was coupled to a Photonis Cricket™ image intensifier, allowing for single-photon detection [34]. The Cricket™ offers a quantum efficiency of 30% and a typical gain of 800,000. The gain of the image intensifier is set using a control voltage, which can be varied between 0–5 V; the minimal background noise in this application being found to be at a voltage of 135 mV. To minimise noise due to light contamination, the sensor was placed within a light-tight box, in a position where it could be imaged by the camera, as can be seen in Figure 4. Initially, a 6 mm wide-angle lens was used to observe the scintillator. This was effective, but was replaced with a macro lens composed of two identical lenses (equivalent aperture  $f/2$ ) placed back-to-back [35]. This led to a significant increase in light collection from the scintillator.

## 5 Detector Performance

The scintillator was exposed to radioactive sources including  $^{90}\text{Sr}$ ,  $^{137}\text{Cs}$  and  $^{252}\text{Cf}$ , allowing for tests of its response to  $\beta$ ,  $\gamma$  and neutrons. The scintillating block was placed 10 cm from the sources, in line with the camera lens. The  $^{90}\text{Sr}$  and  $^{137}\text{Cs}$  source were used with no additional items in the light-tight box. The californium source, meanwhile, was contained in a 5 cm thick lead jacket, with a 10 cm High-Density Poly-Ethylene (HDPE) thermalizer between it and the scintillator. When a combination of  $\gamma$  and neutrons was required, the  $^{137}\text{Cs}$  source was also placed behind the thermalizer, alongside the  $^{252}\text{Cf}$  source. These configurations were simulated using the Geant4 Monte Carlo package, which showed that the thermalizer and lead jacket would create a neutron spectrum with two components; a fast component with energies at around 1 MeV and a slow component with energies at around 0.03 eV [36]. The fast component dominated, with 70% of the neutrons, but the slow component was still significant, containing 20% of the neutrons, allowing us to test the scintillator's sensitivity to both the fast and thermal neutron components.



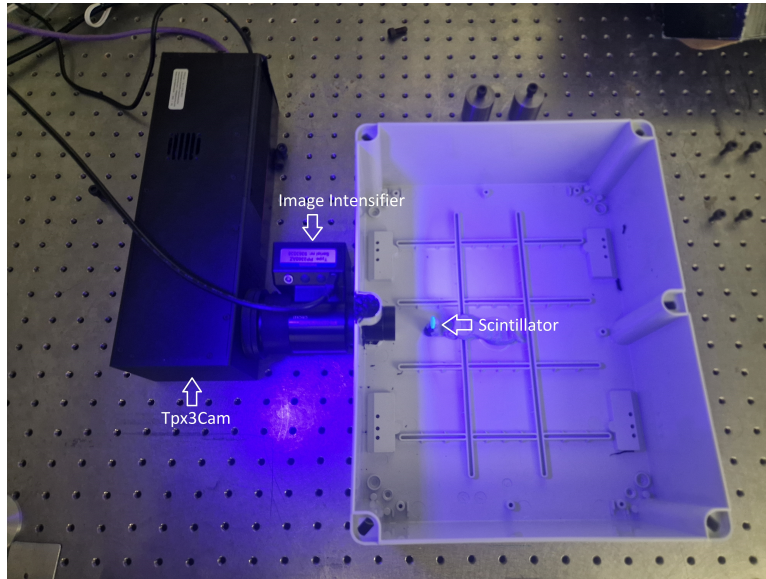


**Figure 4:** The detector system, illuminated with UV light to show the position of the scintillator. The TPX3Cam is on the left, with the image intensifier connected to it. The scintillator is within the light-tight box, glowing under the UV light.

Furthermore, observations of the  $^{90}\text{Sr}$  source were used to determine the optimal composition of the scintillator, testing concentrations of PTP and POPOP between 0-4% for the former and 0-0.1% for the latter. As described above, maximum light output with minimum opacity was found to be given with a concentration of 2% PTP and 0.05% POPOP. The  $^{90}\text{Sr}$  and  $^{137}\text{Cs}$  source were then used to determine the detection performance of the scintillator. It was found that the 3D printed materials had a strong sensitivity to both  $\beta$  and  $\gamma$ . The highest light output was found to be  $30 \pm 5$  photons/MeV. This light output is about  $10^4$  times lower than that of NaI. However, the decay time of the emission is significantly shorter [37].

Measurements of  $^{252}\text{Cf}$  were carried out with two different configurations of printed scintillator: a cuboid, and one with a cavity packed with  $^6\text{Li}$ . The characteristic emission of the latter can be seen in Figure 5a. These were compared with a commercially produced neutron-sensitive scintillator, Eljen Technology's EJ-420 [38]. All three scintillators displayed sensitivity to neutrons, with a significant increase in photo-emission over the noise level. The EJ-420 scintillator, however, was found to be more sensitive than the 3D-printed cuboid, with 4.5 times more detections. The scintillator with the increased Li content was, as expected, more sensitive than the cuboid, increasing detections by a factor of 2.

## 5.1 Neutron-Gamma Discrimination

The use of the TPX3cam allows a method for neutron-gamma discrimination, without having to tune the scintillator for pulse-shape discrimination. As noted in Section 3, a neutron interaction with  $^6\text{Li}$  will release more energy than that carried by the typical gamma-ray. As such, when the alpha particle and tritium nucleus are detected within the scintillator, a brighter pulse will be emitted. At a basic level, a neutron interaction within the scintillator will cause the emission of

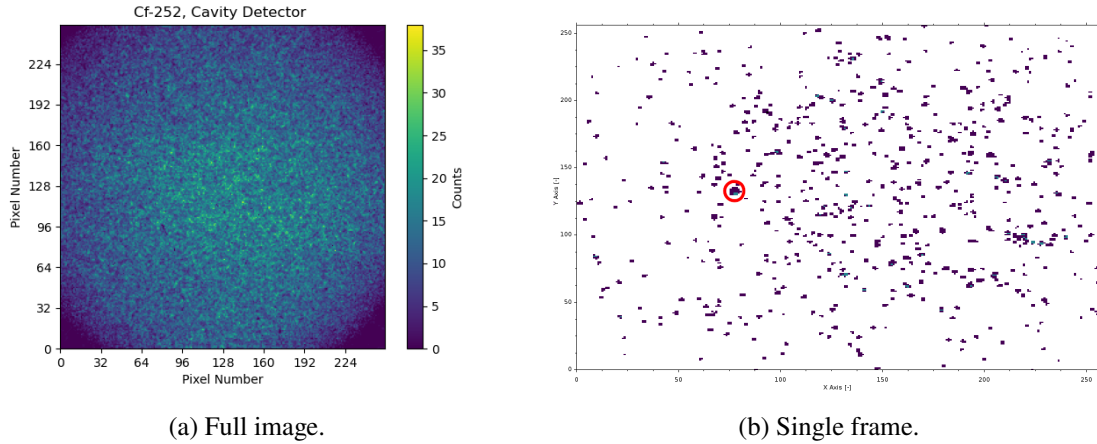
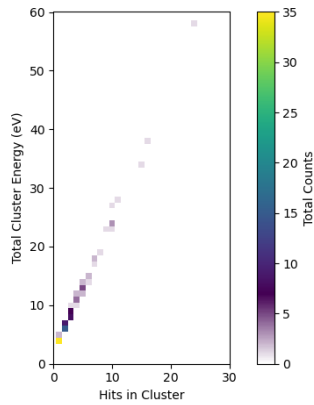


**Figure 5:** Two TimePix images of the 3D-printed lithium-packed scintillator, when exposed to a  $^{252}\text{Cf}$  source. Figure 5a shows a post-processed and summed image, combining multiple such frames from a 30 minute observation. Note the bright central spot, from the scintillator. Figure 5b, meanwhile, is a single raw output frame, using a 0.5 s integration time, and shows a single neutron-associated photon cluster to the left of the centre, in the red circle.

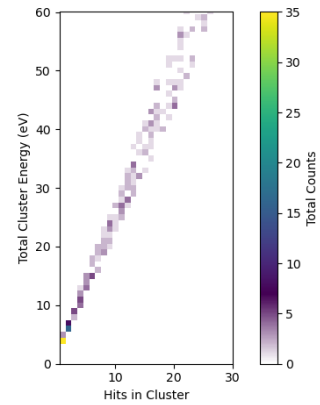
a minimum of 143 photons. For gamma rays with a comparable energy to the alpha particle, the photons will be emitted over a broader area, resulting in a more diffuse pulse. The compact, bright pulse from the detection of an alpha particle will be visible as a large cluster in the TimePix output. By identifying the signature of these larger clusters, we can use this to count individual neutron detections. A cluster is defined as a number of hits within a radius of three TimePix pixels within a time resolution of 100 ns; this was chosen as it matches the decay time of the phosphors in the image intensifier. An example of these clusters can be seen in Figure 5b. By summing the total photon energy for each cluster, we can use this as a proxy for the energy of the incoming particle. In the case of the TimePix, this is in the form of a Time over Threshold (ToT), in nanoseconds.

This was tested with Geant4 simulations of the scintillator, using both thermal neutrons and 662 keV gamma rays. Photons leaving the scintillator and crossing a collector plane were counted, and assigned to clusters, using both time and spatial correlations. The total photon energy was plotted against the total number of collected photons. This showed a clear difference between gamma rays and neutrons, with the neutrons having a 'tail' containing significantly more events, as can be seen in Figure 6. This result was also obtained with the 3D printed scintillator, using the  $^{137}\text{Cs}$  and  $^{252}\text{Cf}$  sources to produce gamma-only and neutron-only signals. The results of this can be seen in Figure 7, which shows a clear cut-off in the gamma-ray data at 5 hits per cluster. By setting a minimum value at 5 hits, we are thus able to draw a distinction between neutrons and gamma rays. Based on this, we can plot a cluster energy spectrum for both simulated data and for the real scintillator. Both show a similar peak, associated with thermal neutrons, shown in Figure 8.

This method, as it relies on the neutron- $^6\text{Li}$  reaction, is not sensitive to fast neutrons. These can be detected by the scintillator, through proton recoil. However, simulations have shown that proton recoil does not cause the same scintillation signature to which this method is sensitive. As such, this method does not allow for the detection of fast neutrons.

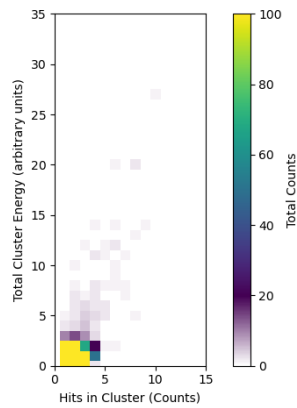


(a) Gamma Rays.

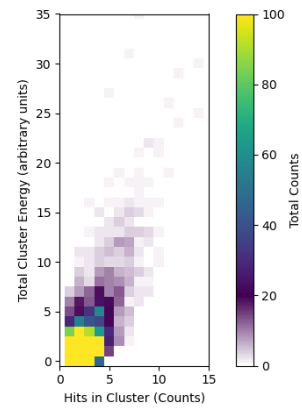


(b) Neutrons.

**Figure 6:** Representations of cluster size against energy for Geant4 simulated particles interacting with a plastic scintillator. Figure 6a) is for a simulation with gamma rays only, while Figure 6b) is for neutrons only. Note that Figure 6b) has a more extensive 'tail', containing more clusters, above 10 photons per cluster, than is seen with gamma rays, confirming that this can be used to distinguish between the two particles.



(a) Gamma Rays.



(b) Neutrons.

**Figure 7:** Experimental data showing of the relationship between cluster size and energy for real particles using the lithium-loaded 3D-printed plastic scintillator. Figure 7a) is for  $^{137}\text{Cs}$  gamma rays only, while Figure 7b) is for  $^{252}\text{Cf}$  neutrons only. Note that the brighter 'tail' seen in Figure 6b) is replicated in Figure 7b). Note also that there are significantly more neutron clusters containing 5 or more hits, making this a useful cut-off for neutron/gamma discrimination. Higher-energy particles create more photons and transfer higher energies, creating the relationship seen here, and allowing for spectral measurements.

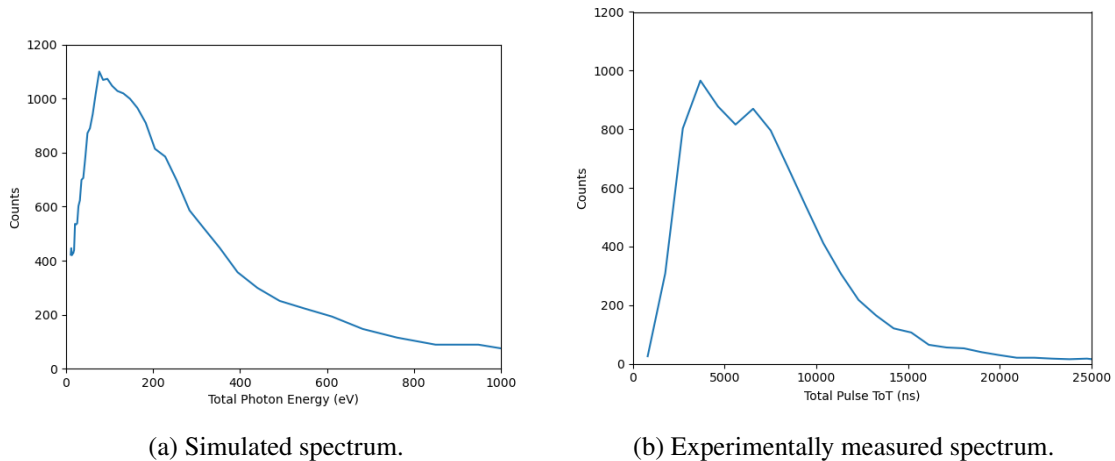


**Figure 8:** Cluster energy spectra, as measured by from simulation (left, 8a) and from experimental measurement (right, 8b). Both show a similar peak, which is associated with the presence of thermal neutrons. A double-peak is seen in both figures, but is more pronounced in Figure 8b. This results from light attenuation within the scintillator.

## 6 Conclusions

This work demonstrates the successful fabrication of a neutron-sensitive scintillating 3D-printed detector via the FDM method, using commercially accessible materials and equipment. The developed scintillator, based on established compounds like Li-6, offers a scalable and rapid production pathway for scintillators. Integration with a fast optical detector system confirmed sensitivity to both ionizing radiation and thermal neutrons, achieving a measured light yield of 30 photons/MeV. Furthermore, a novel neutron/gamma discrimination algorithm was implemented, enabling effective separation of neutron signals from gamma-ray backgrounds, validating the detector’s performance in mixed radiation fields. To improve the performance of the scintillator, we are exploring the use of perovskite materials. This will improve the light output of the scintillator, while preserving the low decay times.

## Acknowledgments

This work was funded by a grant from the Nuclear Security Science Network. A. Barr thanks Paul Campbell and Andy McFarlane for support and assistance with printing, materials and sources.

## References

- [1] M.G. Schorr and F.L. Torney, *Solid non-crystalline scintillation phosphors*, *Phys. Rev.* **80** (1950) 474.
- [2] M. Hamel, *Plastic Scintillators: Chemistry and Applications*, Springer, Switzerland (2021).
- [3] Y. Abreu, Y. Amhis, L. Arnold, G. Ban, W. Beaumont, M. Bongrand et al., *Performance of a full scale prototype detector at the br2 reactor for the solid experiment*, *Journal of Instrumentation* **13** (2018) P05005.

- [4] P. Adragna, C. Alexa, K. Anderson, A. Antonaki, V. Batusov, P. Bednar et al., *The ATLAS Hadronic Tile Calorimeter: From Construction Toward Physics*, *IEEE Transactions on Nuclear Science* **53** (2006) 1275.
- [5] P. Masoliver and A. Abusleme, *Position-sensitive hybrid particle detector based on discrete-time readout*, *Nuclear Instruments and Methods in Physics Research A* **1061** (2024) 169121.
- [6] F. Reines and C.L. Cowan, *Detection of the free neutrino*, *Phys. Rev.* **92** (1953) 830.
- [7] D.M. Gilliam, A.K. Thompson and J.S. Nico, *A Neutron Sensor for Detection of Nuclear Materials in Transport*, in *Unattended Radiation Sensor Systems for Remote Applications*, J.I. Trombka, D.P. Spears and P.H. Solomon, eds., vol. 632 of *American Institute of Physics Conference Series*, pp. 291–294, AIP, Oct., 2002, DOI.
- [8] U. Bravar, P.J. Bruillard, E.O. Flckiger, J.R. Macri, M.L. McConnell, M.R. Moser et al., *Design and Testing of a Position-Sensitive Plastic Scintillator Detector for Fast Neutron Imaging*, *IEEE Transactions on Nuclear Science* **53** (2006) 3894.
- [9] R.C. Runkle, A. Bernstein and P.E. Vanier, *Securing special nuclear material: Recent advances in neutron detection and their role in nonproliferation*, *Journal of Applied Physics* **108** (2010) 111101.
- [10] J.B. Birks, *The scintillation process in organic systems*, *IRE Transactions on Nuclear Science* **7** (1960) 2.
- [11] M. Koshimizu, *Fundamental processes and recent development of organic scintillators*, *Journal of Luminescence* **278** (2025) 121008.
- [12] Y. Yoshimura, T. Inagaki, T. Morimoto, I. Sugai, M. Kuriki, R. Shirai et al., *Plastic scintillator produced by the injection-molding technique*, *Nuclear Instruments and Methods in Physics Research Section A: Accelerators, Spectrometers, Detectors and Associated Equipment* **406** (1998) 435.
- [13] J. Thevenin, L. Allemand, E. Locci, P. Micolon, S. Palanque and M. Spiro, *Extruded polystyrene, a new scintillator*, *Nuclear Instruments and Methods* **169** (1980) 53.
- [14] X. Zheng, J. Deotte, M.P. Alonso, G.R. Farquar, T.H. Weisgraber, S. Gemberling et al., *Design and optimization of a light-emitting diode projection micro-stereolithography three-dimensional manufacturing system*, *Review of Scientific Instruments* **83** (2012) 125001.
- [15] Stratasys, *FDM Technology*, 2025. <https://www.stratasys.com/en/guide-to-3d-printing/technologies-and-materials/FDM-technology/>.
- [16] Y. Mishnayot, M. Layani, I. Cooperstein, S. Magdassi and G. Ron, *Three-dimensional printing of scintillating materials*, *Review of Scientific Instruments* **85** (2014) 085102.
- [17] Y. Kim, N. Zaitseva, M.J. Ford, L. Carman, A. Glenn, M. Febbraro et al., *3D printable polyvinyltoluene-based plastic scintillators with pulse shape discrimination*, *Nuclear Instruments and Methods in Physics Research A* **1055** (2023) 168537.
- [18] P. Stowell, Z. Kutz, S. Fargher and L. Thompson, *3D Printing Neutron Detectors using Scintillating BN/ZnS Resin*, *Journal of Instrumentation* **16** (2025) .
- [19] M. Hamel and G. Lebouteiller, *Attempting to prepare a plastic scintillator from a biobased polymer*, *Journal of Applied Polymer Science* **137** (2020) 48724 [<https://onlinelibrary.wiley.com/doi/pdf/10.1002/app.48724>].
- [20] S. Berns, A. Boyarintsev, S. Hugon, U. Kose, D. Sgalaberna, A.D. Roeck et al., *A novel polystyrene-based scintillator production process involving additive manufacturing*, *Journal of Instrumentation* **15** (2020) P10019.

- [21] S. Berns, E. Boillat, A. Boyarintsev, A.D. Roeck, S. Dolan, A. Gendotti et al., *Additive manufacturing of fine-granularity optically-isolated plastic scintillator elements*, *Journal of Instrumentation* **17** (2022) P10045.
- [22] T. Sibilieva, V. Alekseev, S. Barsuk, S. Berns, E. Boillat, I. Boiaryntseva et al., *3D printing of inorganic scintillator-based particle detectors*, *Journal of Instrumentation* **18** (2023) P03007.
- [23] B. Li, T. Weber, U. Kose, M. Franks, J. Wüthrich, X. Zhao et al., *Beam test results of a fully 3D-printed plastic scintillator particle detector prototype*, *Journal of Instrumentation* **20** (2025) P04008 [2412.10174].
- [24] D. Chiesa, M. Nastasi, C. Cazzaniga, M. Rebai, L. Arcidiacono, E. Previtali et al., *Measurement of the neutron flux at spallation sources using multi-foil activation*, *Nuclear Instruments and Methods in Physics Research A* **902** (2018) 14 [1803.00605].
- [25] F.D. Brooks, *A scintillation counter with neutron and gamma-ray discriminators*, *Nuclear Instruments and Methods* **4** (1959) 151.
- [26] R. Breukers, C. Bartle and A. Edgar, *Transparent lithium loaded plastic scintillators for thermal neutron detection*, *Nuclear Instruments and Methods in Physics Research Section A: Accelerators, Spectrometers, Detectors and Associated Equipment* **701** (2013) 58.
- [27] N. Zaitseva, A. Glenn, H. Paul Martinez, L. Carman, I. Pawelczak, M. Faust et al., *Pulse shape discrimination with lithium-containing organic scintillators*, *Nuclear Instruments and Methods in Physics Research A* **729** (2013) 747.
- [28] Sigma Aldrich, *Polystyrene*, 2025. <https://www.sigmaaldrich.com/GB/en/product/aldrich/430102>.
- [29] 3devo B.V., *Filament Maker ONE*, 2025. <https://www.3devo.com/filament-maker-one-composer-precision>.
- [30] Prusa Research a.s., *Original Prusa i3 MK3*, 2025. <https://help.prusa3d.com/product/mk3>.
- [31] Amsterdam Scientific Instruments, *TPX3Cam*, 2025. <https://amscins.com/>.
- [32] G. D'Amen, M. Keach, A. Nomerotski, P. Svihra and A. Tricoli, *Novel imaging technique for  $\alpha$ -particles using a fast optical camera*, 2020. <https://arxiv.org/abs/2010.15185>.
- [33] A. Nomerotski, M. Chekhlov, D. Dolzhenko, R. Glazenborg, B. Farella, M. Keach et al., *Intensified tpx3cam, a fast data-driven optical camera with nanosecond timing resolution for single photon detection in quantum applications*, *Journal of Instrumentation* **18** (2023) C01023.
- [34] Exosens, *Photonis Cricket*, 2025. <https://www.exosens.com/products/crickettm2>.
- [35] T. Gao, M. Alsulimane, S. Burdin, G. DAmen, C.D. Via, K. Mavrokoridis et al., *Feasibility study of a novel thermal neutron detection system using event mode camera and lyso scintillation crystal*, 2024. <https://arxiv.org/abs/2411.12095>.
- [36] S. Agostinelli, J. Allison, K. Amako, J. Apostolakis, H. Araujo, P. Arce et al., *Geant4—a simulation toolkit*, *Nuclear Instruments and Methods in Physics Research A* **506** (2003) 250.
- [37] G.F. Knoll, *Radiation Detection and Measurement*, Wiley, Hoboken, New Jersey, United States of America (2010).
- [38] Eljen Technology, *Ej-420*, 2025. <https://eljentechnology.com/products/neutron-detectors/ej-420>.